Microwave and Millimeter-Wave QWITT Diode Oscillators

VIJAY P. KESAN, MEMBER, IEEE, AMIR MORTAZAWI, STUDENT MEMBER, IEEE, DOUGLAS R. MILLER, VIJAY K. REDDY, DEAN P. NEIKIRK, MEMBER, IEEE, AND TATSUO ITOH, FELLOW, IEEE

Abstract—**We present dc, microwave, and millimeter-wave characteristics of different quantum well injection transit time (QWITT) devices. Small-signal and large-signal device models are used to provide physical device design parameters to maximize the output power density at any desired frequency of operation. A peak output power density of 3.5–5 kW/cm^2 in the frequency range of 5–8 GHz has been obtained from a planar QWITT oscillator. This is the highest output power density obtained from any quantum well oscillator at any frequency. This result also represents the first planar circuit implementation of a quantum well oscillator. Good qualitative agreement between dc and RF characteristics of QWITT devices and theoretical predictions based on small-signal and large-signal analyses has been achieved. We also present results on improving device efficiency by optimizing the design of the drift region in the device through the use of a doping spike. By optimizing the doping concentration of the spike, an increase in efficiency from 3 to 5 percent has been obtained, without compromising the output power at X-band. Self-oscillating QWITT diode mixers have also been demonstrated at X-band in both waveguide and planar circuits. The self-oscillating mixer exhibits a conversion gain of about 10 dB in a narrow bandwidth and a conversion loss of about 5 dB if broad-band operation is desired. This is to our knowledge the first report of conversion gain obtained from a self-oscillating mixer using a quantum well device.**

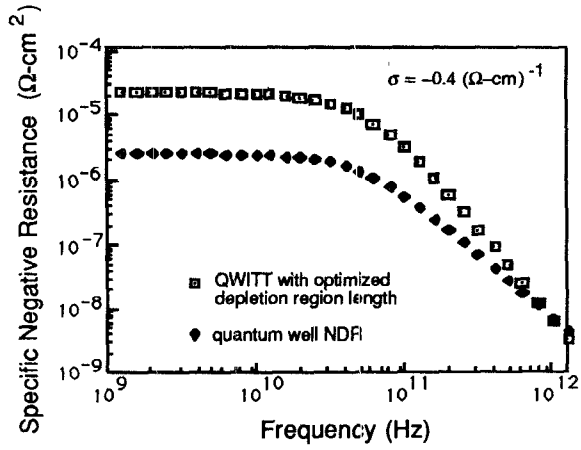

Fig. 1. Predicted small-signal specific negative resistance as a function of frequency for a QWITT diode and a resonant tunneling diode. Note the broad-band nature of the specific negative resistance and the high frequency f^{-2} roll-off.

I. INTRODUCTION

QUANTUM WELL oscillators have been shown to be capable of generating power at high millimeter-wave frequencies [1]–[5], and there is great expectation that these devices will serve as useful local oscillators at frequencies between 100 and 1000 GHz. However, the output power obtained from these devices, thus far, has been rather low. The physical device structures that must be used to maximize the output power density obtained from these devices remain to be explored fully.

We have proposed an improved quantum well oscillator, the quantum well injection transit time (QWITT) diode [6], consisting of a double barrier structure coupled with a depletion region or drift region. Such a device, when biased in the negative differential resistance (NDR) regime of its $I-V$ characteristic, has a broad-band negative resistance which is essentially constant from dc to a characteristic frequency $\omega_0 = |\sigma|/\epsilon$, where σ is the slope of the dc $J-E$ curve of the quantum well region about the dc bias point [7]. For frequencies below ω_0, the presence of a depletion region increases the voltage swing between peak and valley, thus increasing the dc specific negative resistance obtained from the device. Note that for frequencies below ω_0, transit *time* effects are not important, although depletion region transport can still lead to significant increases in negative resistance. At low frequency the optimum depletion region length is independent of frequency, depending primarily on σ and the depletion region saturation velocity [7]. For frequencies beyond ω_0, transit time effects become important and the optimum drift region length does depend on frequency. In addition, at frequencies above ω_0, the specific negative resistance of a device with optimum drift region length rolls off as the square of the frequency. Fig. 1 shows a plot of small-signal specific negative resistance as a function of frequency for optimized QWITT devices [7]. It is important to note that this broad-band negative resistance is very different from

Manuscript received March 31, 1989; revised July 12, 1989. This work was supported by the Joint Services Electronics Program under AFOSR F 49620-86-C-0045 and by the Texas Advanced Technology Program.

V. P. Kesan was with the Department of Electrical and Computer Engineering, University of Texas at Austin, Austin, TX 78712. He is now with the IBM T. J. Watson Research Center, Yorktown Heights, NY 10598.

A. Mortazawi, D. R. Miller, V. K. Reddy, D. P. Neikirk, and T. Itoh are with the Department of Electrical and Computer Engineering, University of Texas at Austin, Austin, TX 78712.

IEEE Log Number 8930810.

0018-9480/89/1200-1933$01.00 ©1989 IEEE

the narrow-band specific negative resistance commonly seen for other transit time devices. This is due to the fact that the injection region itself (i.e., the quantum well) possesses negative differential resistance. Also shown is the calculated specific negative resistance obtained from a double barrier quantum well structure with no depletion region on the anode side. We can clearly see that by an appropriate choice of a depletion region on the anode side of the device an increase in specific negative resistance, and hence RF output power, can be obtained. We have performed both small- and large-signal analyses [7]–[9] of the QWITT diode in order to develop a model that relates physical device and material parameters to the RF performance of the device. These models can be used to design an improved device structure for a given frequency of operation.

There is also increasing interest in developing quantum well (QW) devices for millimeter-wave technology beyond source applications [10]. Since the QWITT diode is a highly nonlinear negative resistance device, and due to the fact that quantum mechanical tunneling is an intrinsically low-noise phenomenon, self-oscillating QWITT diode mixers could be expected to possess some conversion gain with a low noise figure. Therefore, the QWITT diode has the potential of being used as a self-oscillating mixer.

This paper presents dc and RF results for microwave and millimeter-wave QWITT diode oscillators in both planar and waveguide resonant circuits. Two different types of QWITT structures are studied: (a) devices with a uniformly doped drift region and (b) devices with a doping spike at the beginning of the drift region. The dc and RF characteristics are compared to predicted behavior based on small-signal and large-signal models for the device. Preliminary experimental results using the QWITT diode as a waveguide self-oscillating harmonic mixer and also as a planar self-oscillating mixer operating in the fundamental mode are also presented.

II. Experiment

The heterolayers used in this study were grown in a Varian GEN II MBE system on n^+ (3–5×10^{18} cm^{-3} Si-doped) (100) GaAs substrates. A schematic diagram of the device structures used in this study is shown in Fig. 2. Three QWITT device structures, A, B, and C, consisting of identical quantum well regions but with three different n^- (5×10^{16} cm^{-3} Si-doped) GaAs drift region lengths of 500, 1000, and 2000 Å, respectively, were examined [11]. A maximum depletion region length of 2000 Å was chosen, since that corresponds to the optimum length of the drift region for 10 GHz operation based on the small-signal model for the QWITT diode [7]. The quantum well regions consisted of a 50 Å GaAs layer sandwiched between two AlAs layers 17 Å thick. The AlAs barrier layers were kept thin to increase the current density through the device, and to also promote Γ(GaAs)–Γ(AlAs) tunneling [12]. Due to the large Γ(GaAs)–Γ(AlAs) conduction band discontinuity of 1.1 eV in this material system, increased Γ(GaAs)–Γ(AlAs) tunneling, as seen in thin AlAs barriers,

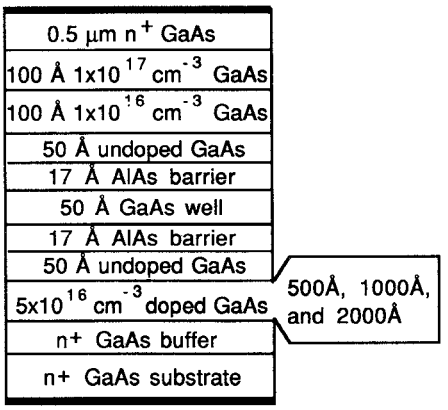

Fig. 2. A schematic cross section of the QWITT diode structures, A through D, examined in this study.

has been shown to produce improved peak-to-valley current ratios from GaAs–AlAs resonant tunneling diodes [13]. A 250-Å-thick GaAs spacer region consisting of a 100 Å n-type (1×10^{17} cm^{-3} Si-doped) layer, followed by a 100 Å n-type (1×10^{16} cm^{-3} Si-doped) layer with a 50 Å unintentionally doped p-type ($\sim1\times10^{14}$ cm^{-3}) layer, was used on the cathode side of the devices (Fig. 2). In addition, a baseline resonant tunneling diode structure, D, with the same quantum well layers and with the same 250 Å GaAs spacer layer on either side of the device was grown. Device mesas were defined using conventional photolithography and wet etching techniques. Device diameters were typically 4–8 μm, corresponding to a device area of 1.25–5×10^{-7} cm^2. Continuous and pulsed (50 percent duty cycle) dc current–voltage characteristics at room temperature were measured.

For QWITT devices containing a uniformly doped depletion region, our self-consistent large-signal model [9] indicates that the electric field in this region is of the order of 100 kV/cm. For GaAs, electric fields around 3–10 kV/cm are sufficient to have carrier velocities around 10^7 cm/s. Hence, a doping spike at the beginning of the drift region could be introduced, much like that in a lo–hi–lo IMPATT structure [14], so that the electric field in the GaAs drift region is reduced, and yet the entire drift region is fully depleted. This should result in a reduction in the dc bias across the device and hence improve the dc-to-RF conversion efficiency. Since the entire drift region is still depleted, the voltage swing between peak and valley would remain the same, and thus the RF output power would not be reduced compared to the uniformly doped drift region device. Fig. 3 shows the schematic of the device structures, E through H, examined in this study. Device E corresponds to the limiting case where the doping concentration in the spike equals the background doping of 5×10^{16} cm^{-3} in the drift region. Devices F through H contain a 100 Å GaAs doping spike of varying Si doping concentration from 8×10^{16} cm^{-3} to 5×10^{17} cm^{-3} at the beginning of the drift region followed by a 1800 Å n-type GaAs layer (5×10^{16} cm^{-3} Si-doped). Note that the total thickness of the GaAs layers following the quantum

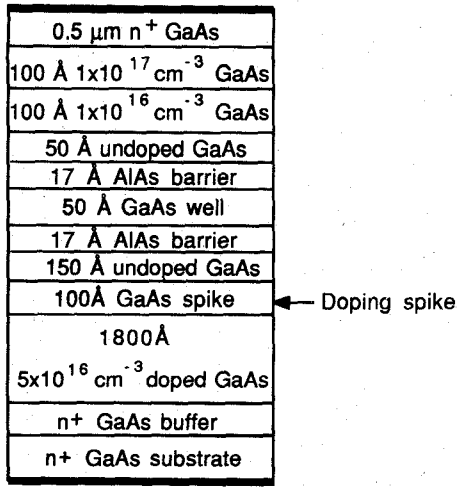

Fig. 3. A schematic cross section of the QWITT diode structures with a doping spike, E through H, examined in this study; the Si doping in the spike was varied between 5×10^{16} and $5\times10^{17}\,cm^{-3}$.

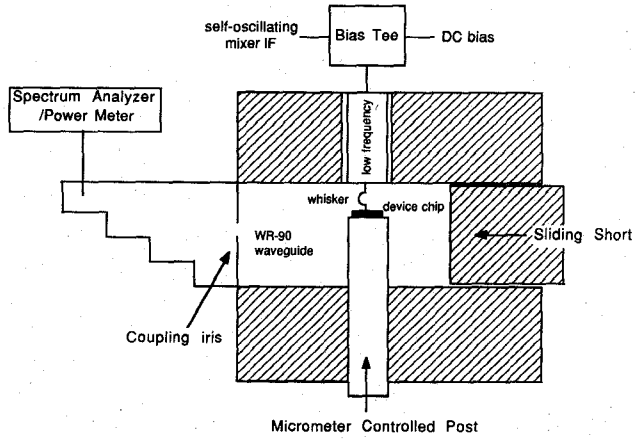

Fig. 4. Block diagram of the waveguide circuit used at microwave and millimeter-wave frequencies.

well region on the anode side is constant at 2000 Å for devices C and E through H (Figs. 2 and 3). Device structures A through H all have identical quantum well regions and cathode spacer levels.

Microwave and millimeter-wave waveguide oscillators were implemented using the QWITT devices described above. The devices were mounted in WR-90 (8–12 GHz) and WR-22 (33–50 GHz) waveguides using a micrometer-controlled post and whisker-contacted for microwave and millimeter-wave measurements. A block diagram of the waveguide oscillator measurement setup is shown in Fig. 4. On one end of the waveguide a sliding short is used to modulate the impedance of the waveguide circuit to obtain the highest output power. On the other end the waveguide is coupled to a spectrum analyzer or power meter. The dc bias to the diode is provided through a bias tee to obtain dc and RF isolation. It is important to avoid low-frequency oscillations in the dc bias circuit due to the intrinsic broad-band negative resistance characteristics of a QWITT diode. In addition a planar microstrip oscillator circuit was designed using a standard microwave CAD package,

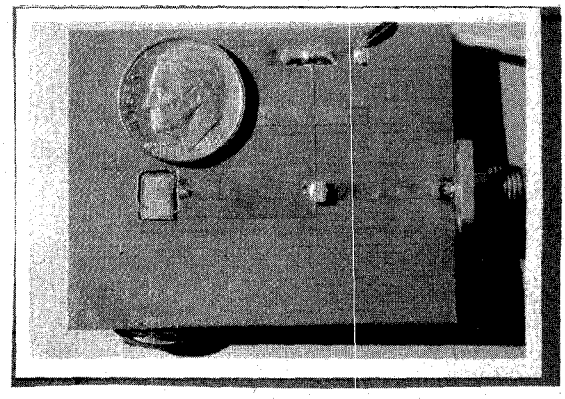

(a)

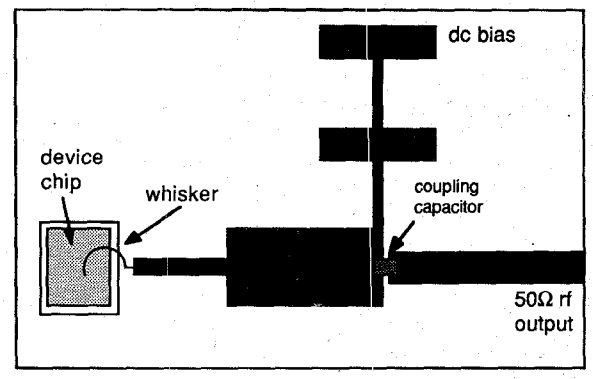

(b)

Fig. 5. (a) Photograph of a planar microstrip QWITT diode oscillator at *X*-band. (b) Schematic layout of the circuit shown in (a).

Touchstone [15], to match the QWITT diode impedance as predicted by the large-signal model [8]. Fig. 5 shows a photograph of the 10 GHz planar microstrip oscillator used. A lo–hi–lo impedance transformer was used to bias the diode and obtain dc and RF isolation at the bias point. Chip capacitors were used to block the dc signal at the RF output. Contact to one device is achieved using a small whisker, whose inductive contribution was included in the planar circuit design. This circuit (Fig. 5(a) and (b)) represents the first planar implementation of a quantum well oscillator. The output power measurements for the QWITT oscillator were verified independently using a spectrum analyzer and an RF power meter.

III. Results and Discussion

A. DC Characteristics

Table I shows the room-temperature dc $I-V$ characteristics obtained from devices A through D. The QWITT bias direction corresponds to electron injection from the top contact. The $I-V$ characteristics in either bias direction for sample D are quite symmetric with a typical peak-to-valley current ratio of 2–3:1 and a peak current density of around 20 kA/cm^2. Due to the asymmetric structure of the QWITT diode (structures A through C), the dc $I-V$ characteristics for the two bias directions are very different. In any negative resistance diode the voltage and current differences between peak and valley, ΔV_{pv} and ΔI_{pv}, must be

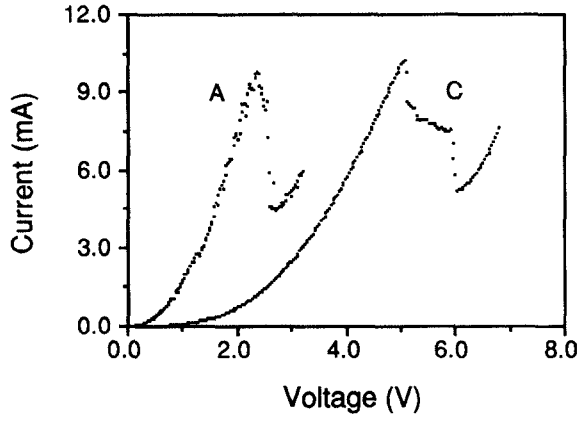

Fig. 6. Room-temperature dc $I-V$ curves for QWITT devices A and C with 500 Å and 2000 Å depletion region lengths, respectively.

TABLE I
DC CHARACTERISTICS FOR QWITT DEVICES WITH UNIFORMLY DOPED DEPLETION REGIONS, A THROUGH D

Structure	V_p (V)	ΔV (V)	J_p kA/cm^2	ΔJ kA/cm^2	peak to valley ratio	Specific Negative Resistance Ω-cm^2
(A) 50Å spacer W = 500Å 5x10^{16}	2.5	0.3	26	12	1.8	2.6 x 10^{-5}
(B) 50Å spacer W = 1000Å 5x10^{16}	4.6	0.5	30	13	1.8	3.9 x 10^{-5}
(C) 50Å spacer W = 2000Å 5x10^{16}	5.1	1.0	28	14	2.0	6.8 x 10^{-5}
(D) symmetric RTD	0.88	0.34	20	11	2.3	3.1 x 10^{-5}

W is the depletion layer thickness, V_p is the peak voltage, ΔV is the peak-to-valley voltage difference, J_p is the peak current density and ΔJ is the peak-to-valley current density difference.

as large as possible to increase the device output power; in a low frequency model (i.e., frequency below $\omega_0 = |\sigma|/\epsilon$), maximum output power should be proportional to $\Delta V_{pv} \cdot \Delta I_{pv}$. For the QWITT diode, ΔV_{pv} is increased through the use of a drift region, but ΔI_{pv} should remain virtually the same as in the intrinsic quantum well. This results in an increase in the total output power that can be obtained from the QWITT diode compared to a bare resonant tunneling diode. For the QWITT bias mode (forward bias, substrate positive), as the length of the drift region is increased from 500 to 2000 Å, the voltage corresponding to the current peak, V_p, increases from 2.5 to 5.1 V, and the voltage difference between peak and valley currents, ΔV_{pv}, also increases from 0.3 to 1.0 V (Fig. 6 and Table I). We can see that while the variation in peak-to-valley current differences, ΔJ_{pv}, and peak current density, J_p, for the three devices A, B, and C is quite small, large differences in ΔV_{pv} are observed (Table I). Devices A and D have very similar voltage swings, ΔV_{pv}, since the length of the depletion region in both these structures is almost the same. The increase in ΔV_{pv} obtained through a proper choice of the depletion region length also results in a corresponding increase in the specific negative resistance ($\Delta V_{pv}/\Delta J_{pv}$) of the device. This suggests that the best oscillator performance in terms of output power would be obtained from device C. For this quantum well structure, when the depletion region length is increased much beyond 2000 Å, the small-signal and large-signal analyses [7], [9] for the QWITT diode show that the voltage swing between peak and valley, ΔV_{pv}, actually decreases due to the increased positive resistance in the device arising from both the space charge resistance and the undepleted portion of the drift region. This would then result in a degradation in the RF performance of the diode. For each device structure, when electrons are injected from the substrate to the top (reverse bias, substrate negative) ΔV_{pv} is smaller than when electrons are injected from the top to the substrate (forward bias). This is because in reverse bias the n^- GaAs drift region is under accumulation, and can add only positive series resistance to the device, thus reducing ΔV_{pv}. This is in contrast to the QWITT mode, where this region actually contributes to the negative resistance of the device.

A systematic study of the variations in peak voltage and peak current due to both processing conditions and reproducibility of the device structure by MBE was undertaken. We found a 10 percent variation in peak voltage from process-induced changes, arising primarily from variations in the quality of the ohmic contacts, caused by small changes in the AuGe/Ni metallization scheme. InGaAs-based ohmic contacts [16] should significantly improve the ohmic contact reproducibility. Changes in nominally the same device structure from one MBE growth run to another were found to be within the 10 percent change in voltage due to processing variations. We have also found a 20 percent variation in the peak current density arising primary due to inaccuracy in the estimate of the device area.

In devices E through H a doping spike was introduced at the beginning of the drift region to reduce the electric field and thus decrease the dc bias, but yet fully deplete the entire drift region. Table II shows the room-temperature dc $I-V$ characteristics obtained from devices E through H. By changing the doping concentration in the spike from 5×10^{16} cm^{-3} to 5×10^{17} cm^{-3} the peak voltage is reduced from 3.5 V in device E to 0.64 V in device H. However, the voltage swing, ΔV_{pv}, is also reduced from 1.1 to 0.34 V, suggesting that the lightly doped GaAs drift region is not fully depleted. By reducing the spike doping concentration to 1×10^{17} cm^{-3} in device G the voltage swing, ΔV_{pv}, improves to 0.64 V but this value is still lower than that seen in the uniformly doped device E. A further reduction in the spike doping concentration to 8×10^{16} cm^{-3} in device F causes ΔV_{pv} to recover to 1.2 V. Note that the peak voltage in device F is about 30 percent lower than in device E, but the voltage swing, ΔV_{pv}, and the current swing, ΔJ_{pv}, for the two devices are similar. This

TABLE II
DC CHARACTERISTICS FOR QWITT DEVICES WITH A DOPING SPIKE, E THROUGH H

Structure	V_p (V)	ΔV (V)	J_p kA/cm^2	ΔJ kA/cm^2	peak to valley ratio	Specific Negative Resistance Ω-cm^2
(E) 100Å spike 5×10^{16} W = 1800Å	3.5	1.1	31	19	2.5	5.8×10^{-5}
(F) 100Å spike 8×10^{16} W = 1800Å	2.6	1.2	28	17	2.6	7.0×10^{-5}
(G) 100Å spike 1×10^{17} W = 1800Å	0.9	0.64	23	12	2.1	5.3×10^{-5}
(H) 100Å spike 5×10^{17} W = 1800Å	0.64	0.34	21	12	2.3	2.8×10^{-5}

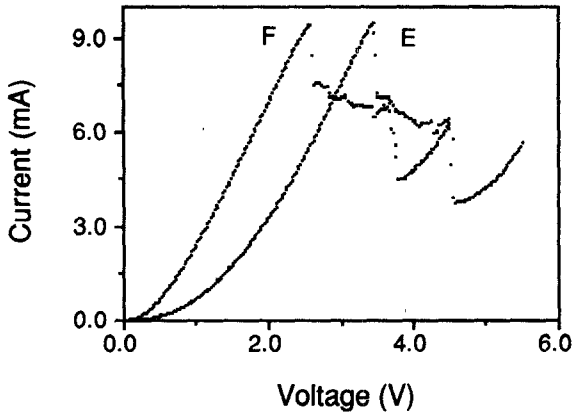

Fig. 7. Room-temperature dc $I-V$ curves for QWITT devices E and F with a Si doping spike of 5×10^{16} cm^{-3} and 1×10^{17} cm^{-3}, respectively.

suggests that the oscillator output power obtained from devices E and F should be the same, with device F having a higher efficiency due to the lower dc bias obtained through the introduction of a doping spike. The room-temperature dc $I-V$ curves for devices E and F are shown in Fig. 7. As seen before in devices A through C, in the opposite bias direction when the drift region is under accumulation the increased series resistance in the device causes a reduction in the voltage swing, ΔV_{pv}.

In conclusion, dc characteristics of different QWITT devices with both uniformly doped drift regions and with drift regions containing a doping spike have been presented. In order to obtain the best RF oscillation performance the importance of choosing a device structure that maximizes the $\Delta V_{pv}\cdot\Delta I_{pv}$ product, is emphasized. As will be seen in the next section when characterizing QWITT diode oscillators at frequencies below the characteristic frequency, $|\sigma|/2\pi\epsilon$ (this frequency is typically around 40 GHz for $|\sigma| = 0.3$ mho/cm), the dc characteristics are a good measure of RF oscillator performance. This is consistent with the small-signal analysis for the QWITT diode [7], where we found that the specific negative resistance for a QWITT diode is essentially constant from dc up to frequencies around $|\sigma|/2\pi\epsilon$.

TABLE III
MICROWAVE AND MILLIMETER-WAVE PERFORMANCE OF QWITT DIODE OSCILLATORS, A THROUGH D, IN BOTH WAVEGUIDE AND PLANAR CIRCUITS; MEASURED NEGATIVE RESISTANCE AND THAT PREDICTED BY THE SMALL-SIGNAL MODEL [7] ARE ALSO GIVEN

Drift Region Length	Specific Negative Resistance (10^{-5} Ω-cm^2)		Output Power (μW)	Oscillation Frequency (GHz)
	Measured	Simulation		
500 Å (A)	2.6	2.4	3 240 (planar) 275 (planar)	8-12 6-8 6-8
1000 Å (B)	3.9	3.7	10	8-12
2000 Å (C)	6.8	5.9	30 30 910 (planar)	8-12 28-31 6-8
Symmetric RTD (D)	3.1	2.7	1	8-12

TABLE IV
MICROWAVE AND MILLIMETER-WAVE PERFORMANCE OF QWITT DIODE OSCILLATORS, E THROUGH H, IN PLANAR MICROSTRIP CIRCUITS

Doping Spike	Output Power (μW)	Efficiency	Oscillation Frequency (GHz)
uniform 5×10^{16} (E)	850	3.5%	5-8
8×10^{16} (F)	1000	5.0%	5-8
1×10^{17} (G)	350	4.3%	5-8
5×10^{17} (H)	100	3%	5-8

B. Microwave and Millimeter-Wave Oscillator

The microwave and millimeter-wave performances of different QWITT device structures, A through H, are summarized in Tables III and IV. For each device in the waveguide circuit the output power was a strong function of the position of the sliding short, while the oscillation frequency was only weakly dependent on it. The oscillation frequency was governed by the impedance of the diode and the dc bias point. We can see from Table III that, for devices with the same quantum well structure, as the length of the drift region is increased from 500 to 2000 Å, the output power at X-band in the waveguide circuit increases from 3 to 30 μW. The devices were also mounted in the planar microstrip circuit shown in Fig. 5. With this microstrip circuit oscillations in the frequency range of 6–8 GHz were detected, with a peak output power of ~1 mW from device C. This corresponds to an output power density of 3.5–5.0 kW/cm^2 for a device area of $2\text{–}3.5\times10^7$ cm^2 (5–6 μm in diameter). This result is the highest output power obtained from any quantum well oscillator at any frequency and shows approximately five times higher power and two to three times higher output power density than reported in the literature [17] for a comparable frequency. This result also represents the first planar circuit implementation of a quantum well oscillator. The impedance of

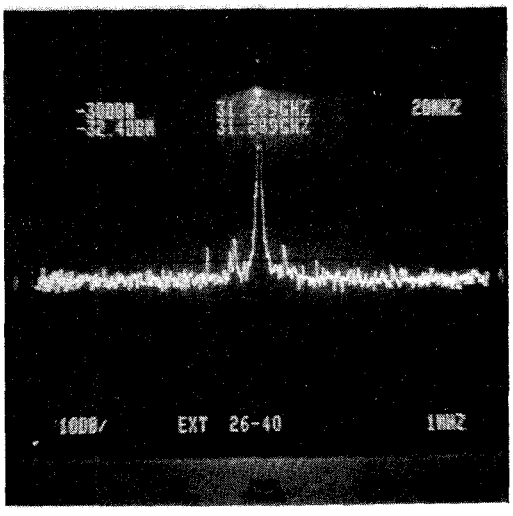

Fig. 8. Spectrum of a QWITT diode (device F) oscillating at 31 GHz in a waveguide circuit.

the planar oscillator circuit is much lower than the full-height waveguide circuit, and the improvement in output power seen in the planar circuit as compared to the waveguide circuit (see Table III) is probably due to a better match to the low impedance of the device. For the different devices, as the length of the drift region is increased from 500 to 2000 Å, the output power increases dramatically in both waveguide and planar oscillator circuits (Table III). The output power at 10 GHz is lower than estimates based on large-signal models for the QWITT diode [8], [18], [19]. This is primarily because the device areas used in this study were not optimized to obtain the highest output power [8] to avoid excessive heating and consequent heat sinking problems. The peak current density in these devices (Table III) is around 25 kA/cm^2. By appropriately choosing the thickness of the quantum well layers the current density can be increased further [20], thus improving the device output power. However, the dramatic increase in output power obtained in devices B and C clearly suggests that, as predicted by the small-signal analysis, the intrinsic device specific negative resistance has been increased through an appropriate choice of drift region length. Further, Table III also shows that at 10 GHz the improvement in RF output power tracks the dc specific negative resistance of the device. This is in keeping with predicted models for the QWITT diode [7], which indicate that the dc $I-V$ curve for the device is a good measure of RF performance at frequencies below $|\sigma|/2\pi\epsilon$ (typically around 40 GHz). Millimeter-wave oscillations in the frequency range 28–31 GHz were obtained in a full-height waveguide circuit from device C with 30 μW output power. Fig. 8 shows a spectrum of a QWITT diode oscillating at 31 GHz in a waveguide resonant circuit. Note that the output power in the WR-22 waveguide circuit at these frequencies (*Ka*-band) is the same as that obtained from the device in the WR-90 waveguide circuit at *X*-band. This indicates that the specific negative resistance of the device has not dramatically changed between 10 and 30 GHz. This is in keeping with the small-signal analysis, which predicts a flat response in specific negative resistance at frequencies below $|\sigma|/2\pi\epsilon$, beyond which the specific negative resistance rolls off as the quantum well capacitance starts to dominate current injection into the drift region.

In order to calculate the specific negative resistance for these devices, the intrinsic injection conductance ($\sigma = \partial J/\partial E$) of the quantum well is determined from the experimental dc $I-V$ characteristics by accounting for the voltage drops in the GaAs spacer regions using a drift/diffusion formalism [9]. For the samples A, B, C, and D, the injection conductance is found to be -0.24, -0.28, -0.20, and -0.15 mho/cm respectively. This value for σ is then used to predict the specific negative resistance for the three devices [7] by assuming a constant carrier velocity in the drift region of 2×10^7 cm/s (Table III). We can see from Table III that the measured specific negative resistance ($\Delta V/\Delta J$) obtained from the dc characteristics of the diode compares well with the predicted values [7].

In devices E through H (see Fig. 3) a doping spike was introduced at the beginning of the drift region to reduce the electric field and thus decrease the dc bias, but yet fully deplete the entire drift region. We can see that in devices G and H the doping concentration in the spike is so high that a large fraction of the drift region is not depleted, causing a reduction in the voltage swing, ΔV_{pv}. This directly translates into lower RF output power for devices G and H, as seen in Table IV. Device E, which is the limiting case of the spike (i.e., a uniformly doped drift region) produces an output power of 850 μW at 3.5 percent efficiency (Table I). Device F is clearly the optimum device since by introducing a 8×10^{16} cm^{-3} doping spike the device efficiency is increased by almost 50 percent compared to device E, with marginally higher output power (1 mW). The RF results obtained from devices C, E, and F represent significant improvement in output power density over previous reports in the literature [17]. Millimeter-wave oscillations in the frequency range 28–31 GHz were also obtained in a full-height waveguide circuit from both devices E and F with 30 μW output power. As before, the output power in the waveguide circuit compared to the microstrip circuit is low due to the poor impedance match between the diode and full-height waveguide.

In summary, microwave and millimeter-wave characteristics of QWITT diode oscillators have been presented. A peak output power of 1 mW, corresponding to an output power density of 3.5–5 kW/cm^2, in the frequency range of 5–8 GHz has been obtained from a planar QWITT oscillator. Millimeter-wave oscillations at 28–31 GHz in a waveguide circuit with an output power of 30 μW have been obtained. In addition, good qualitative agreement between dc and RF characteristics of QWITT devices and theoretical predictions based on small-signal and large-signal analyses has been obtained. We have also presented results in improving device efficiency by optimizing the design of the drift region in the device through the use of a doping spike. By optimizing the doping concentration of the doping spike, an increase in efficiency of from 3 to 5 percent has been obtained, without compromising the output power

at *X*-band. It is clear that there is considerable room for optimization of both the resonant cavity and physical device parameters, including device areas, to maximize RF output power. Nonetheless, the performance achieved here suggests that through further improvements in device and circuit design higher power output may be possible.

C. Self-Oscillating Mixer

We have recently evaluated the potential of a QWITT diode as a self-oscillating mixer [21]. We have realized self-oscillating mixers at *X*-band in waveguide and planar circuits. In the waveguide circuit the QWITT diode is mounted on a micrometer-controlled post which is in electrical contact with the waveguide walls. The dc bias and intermediate frequency connections are provided using a whisker on a metallic post inside the waveguide (see Fig. 4). An *E* and *H* tuner is used to minimize RF reflection and improve the conversion efficiency. The sliding short in the waveguide can also be adjusted to minimize conversion loss. An RF input frequency of 9.3 GHz was chosen in these experiments. A maximum conversion gain of 10 dB was obtained over a narrow bandwidth of 10–20 MHz. The center frequency of the IF signal which results in conversion gain could be varied from the MHz range to about 1 GHz. Broad-band operation (around 100 MHz) was achieved with an average conversion loss of about 5 dB.

The planar self-oscillating mixer uses a microstrip resonant circuit and operates in the fundamental conversion mode. The oscillation frequency of the mixer in this circuit was about 10 GHz. We were able to obtain conversion gains of about 4 dB over a narrow bandwidth of 10–20 MHz. At larger bandwidths (40–200 MHz) conversion losses of about 10 dB with 1.5 dB fluctuations over the entire band were measured.

In summary, self-oscillating QWITT diode mixers have the ability to produce conversion gain at *X*-band. To the best of our knowledge [10] this is the first report of conversion gain obtained from a self-oscillating mixer using a quantum well device.

IV. Conclusion

We have presented dc, microwave, and millimeter-wave characteristics of a QWITT diode oscillator. A peak output power of 1 mW, corresponding to an output power density of 3.5–5 kW/cm^2, in the frequency range of 5–8 GHz has been obtained from a planar QWITT oscillator. This is the highest output power obtained from any quantum well oscillator at any frequency and provides approximately five times higher power and two to three times higher output power density than reported in the literature [17] for a comparable frequency. This result also represents the first planar circuit implementation of a quantum well oscillator. In addition, we have presented results on improving device efficiency by optimizing the design of the drift region in the device through the use of a doping spike. By optimizing the doping concentration of the spike, an increase in efficiency of from 3 to 5 percent is obtained, without compromising output power at *X*-band. Good qualitative agreement between dc and RF characteristics of QWITT devices and theoretical predictions based on small-signal and large-signal analyses is obtained. Millimeter-wave oscillations at 28–31 GHz in a full-height waveguide circuit with an output power of 30 μW have been obtained. We have also demonstrated self-oscillating QWITT diode mixers which have the ability to produce conversion gain at *X*-band. This is to our knowledge the first report of conversion gain obtained from a self-oscillating mixer using a quantum well device.

There is considerable room for optimization of both the resonant cavity and physical device parameters to maximize the oscillator output power. By choosing a InGaAs/InAlAs QWITT structure with high current densities and large peak-to-valley current ratios, even higher output power densities should be realizable. By appropriately choosing the thickness of the quantum well layers the peak current density can be increased further [20], thus improving the device output power. Proper device area optimization [8] will also further enhance the RF output power. It may also be possible to power combine these devices in parallel by periodically loading a parallel-plate waveguide [22], [19]. Nonetheless, the performance achieved here is promising and through further improvements in device and circuit design higher power output may be possible. It seems clear that the actual power limitations of quantum well oscillators have not yet been determined, and that through the use of QWITT design principles useful power levels may be achieved at millimeter-wave frequencies.

Acknowledgment

The authors would like to acknowledge many useful discussions with Dr. B. G. Streetman and Dr. C. M. Maziar.

References

[1] H. Gronqvist *et al.*, "A millimeter wave quantum well diode oscillator," in *Proc. 18th European Microwave Conf.*, (Stockholm, Sweden), Sept. 1988, pp. 370–375.

[2] E. R. Brown, W. D. Goodhue, and T. C. L. G. Sollner, "Fundamental oscillations up to 200 GHz in resonant tunneling diodes and new estimates of their maximum oscillation frequency from stationary-state tunneling theory," *J. Appl. Phys.*, vol. 64, pp. 1519–1529, Aug. 1988.

[3] J.-F. Luy and J. Buechler, "90 GHz SIMMWIC (silicon microwave millimeter wave integrated circuits)," presented at 4th Exhibition and Conf. for Ultra High Frequency Technol., Stuttgart, Germany, 28 Feb. 1989.

[4] I. Song and D. S. Pan, "Efficiency and power output of the quantum-well injection transit-time device," *IEEE Electron Device Lett.*, vol. EDL-8, pp. 560–562, Dec. 1987.

[5] I. Mehdi and G. I. Haddad, "InP based resonant tunneling diodes for millimeter-wave power generation," presented at the Nanostructure Physics and Fabrication Symp., College Station, TX, Mar. 13–15, 1989.

[6] V. P. Kesan, D. P. Neikirk, B. G. Streetman, and P. A. Blakey, "A new transit time device using quantum well injection," *IEEE Electron Device Lett.*, vol. EDL-8, pp. 129–131, Apr. 1987.

[7] V. P. Kesan, D. P. Neikirk, P. A. Blakey, and B. G. Streetman, and T. D. Linton, "Influence of transit time effects on the optimum design and maximum oscillation frequency of quantum well oscillators," *IEEE Trans. Electron Devices*, vol. 35, pp. 405–413, Apr. 1988.

[8] V. P. Kesan *et al.*, "Power-optimized design of quantum well oscillators," in *1987 IEEE Int. Electron Device Meeting Tech. Dig.*, Dec. 6–9, 1987, pp. 62–65.
[9] D. R. Miller, V. P. Kesan, R. L. Rogers, C. M. Maziar, and D. P. Neikirk, "Time dependent simulation of the quantum well injection transit time diode," in *Proc. 13th Int. Conf. Infrared and Millimeter Waves*, Dec. 5–9, 1988, pp. 5–6.
[10] T. C. L. G. Sollner, E. R. Brown, and H. Q. Le, "Microwave and millimeter-wave resonant tunneling devices," *Lincoln Lab. J.*, vol. 1, no. 1, pp. 89–106, Springer 1988.
[11] V. P. Kesan *et al.*, "Microwave frequency operation of quantum-well injection transit time (QWITT) diode," *Electron. Lett.*, vol. 24, pp. 1473–1474, 24, Nov. 1988.
[12] C. S. Kyono, V. P. Kesan, D. P. Neikirk, C. M. Maziar, and B. G. Streetman, "Dependence of apparent barrier height on barrier thickness for perpendicular transport in AlAs/GaAs single barrier structures grown by MBE," *Appl. Phys. Lett.*, vol. 54, no. 6, pp. 549–551, 6 Feb. 1989.
[13] J. Soderstrom and T. G. Andersson, "GaAs/AlAs resonant tunneling diodes: The dependence of the peak-to-valley current ratio on barrier thickness and height," *Superlattices and Microstructures*, vol. 5, no. 1, 1989.
[14] S. M. Sze, *Physics of Semiconductor Devices*, 2nd ed. New York: Wiley, 1981.
[15] TOUCHSTONE, EEsof Inc., Westlake Village, CA.
[16] C. K. Peng, G. Ji, N. S. Kumar, and H. Morkoç, "Extremely low resistance nonalloyed ohmic contacts on GaAs using InAs/InGaAs and InAs/GaAs strained-layer superlattice," *Appl. Phys. Lett.*, vol. 53, no. 10, pp. 900–902, 5 Sept. 1988.
[17] E. R. Brown, T. C. L. G. Sollner, W. D. Goodhue, and C. L. Chen, "High-speed resonant tunneling diodes," in *Proc. SPIE Conf. Quantum Well and Superlattice Physics II*, vol. 943, pp. 2–13, 17–18 Mar. 1988.
[18] I. Song and D. S. Pan, "Analysis and simulation of the quantum-well injection transit-time diode," *IEEE Trans. Electron Devices*, vol. 35, pp. 2315–2322, Dec. 1988.
[19] A. Mortazawi, V. P. Kesan, D. P. Neikirk, and T. Itoh, "Periodic monolithic millimeter-wave quantum well oscillator," in *Proc. 13th Int. Conf. Infrared and Millimeter Waves*, Dec. 5–9, 1988, pp. 47–48.
[20] S. K. Diamond *et al.*, "Fabrication of 200-GHz f_{max} resonant-tunneling diodes for integrated circuit and microwave applications," *IEEE Electron Device Lett.*, vol. 10, pp. 104–106, Mar. 1989.
[21] A. Mortazawi, V. P. Kesan, D. P. Neikirk, and T. Itoh, "A self-oscillating QWITT diode mixer," to be presented at 19th European Microwave Conf., Sept. 1989.
[22] V. P. Kesan, A. Mortazawi, D. P. Neikirk, and T. Itoh, "Monolithic millimeter-wave oscillator using a transmission line periodically loaded by QWITT diodes," *Electron. Lett.*, vol. 24, no. 11, pp. 666–667, 26 May 1988.

Vijay P. Kesan (S'84–M'89) was born in Bombay, India, in 1962. He received the bachelor's degree in electrical engineering from the University of Mysore, India (with highest honors), in 1984 and the M.S. and Ph.D. degrees in electrical engineering from the University of Texas at Austin in 1986 and 1989, respectively. His graduate work included the design, fabrication, and testing of quantum well oscillators for microwave/millimeter-wave applications and MBE growth of III–V heterostructures.

He is presently with the IBM T. J. Watson Research Center, Yorktown Heights, NY, working on silicon-based heterostructure materials and devices.

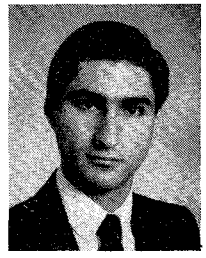

Amir Mortazawi (S'87) was born in Yazd, Iran, on June 7, 1962. He received the B.S. degree in electrical engineering (honors) from the State University of New York at Stony Brook in 1987 and the M.S. degree in electrical engineering from the University of Texas at Austin in 1988, where he is currently working towards the Ph.D. degree. His research interests include solid-state millimeter-wave sources and the nonlinear analysis of microwave devices.

Mr. Mortazawi is a member of Tau Beta Pi, Eta Kappa Nu, and the American Physical Society.

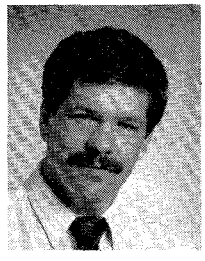

Douglas R. Miller was born in Omaha, NE, on February 5, 1956. He received the bachelor's degree in electrical engineering from the University of Nebraska in 1978, and the master's degree in electrical engineering from the University of Texas in 1988.

In the intervening years, he worked for International Business Machines and the United States Department of Army. He is currently working toward the Ph.D. degree and is a research assistant at the Microelectronic Research Center, University of Texas at Austin. His current research interests include heterostructure device simulation, quantum transport studies, and computational electronics.

Mr. Miller is a member of the American Physical Society.

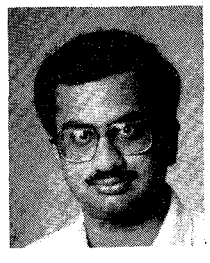

Vijay K. Reddy was born in New Delhi, India, on October 21, 1965. He received the bachelor's degree in electrical engineering from the University of Texas at Austin (with honors) in 1987. He is currently working toward the M.S. degree in the Department of Electrical and Computer Engineering, University of Texas at Austin.

He has been working as a Research Assistant since 1988 in the Microelectronics Research Center, University of Texas at Austin. His research interests include the MBE growth and characterization of resonant tunneling structures for high-frequency millimeter-wave applications and planar microwave integrated circuits.

Mr. Reddy is a member of Tau Beta Pi and the American Physical Society.

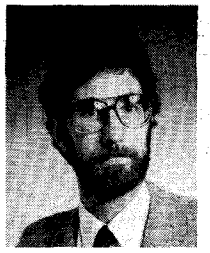

Dean P. Neikirk (S'81–M'83) was born in Oklahoma City, OK, on October 31, 1957. He received the B.S. degree in physics and mathematics from Oklahoma State University in 1979 and the M.S. and Ph.D. degrees in applied physics from the California Institute of Technology in 1981 and 1984, respectively.

He developed the first monolithic, high-resolution focal plane detector array for use at wavelengths between 0.1 and 1 mm. In 1984 he received the Marconi International Fellowship Young Scientist Award for his work in this field. His current research interests concentrate on the use of advanced fabrication techniques, such as molecular beam epitaxy, for millimeter- and submillimeter-wave device development. His work emphasizes novel structures for high-frequency generation, detection, wave guiding, and radiation suitable for monolithic integration. Dr. Neikirk is currently an Associate Professor in Electrical and Computer Engineering at the University of Texas at Austin, and holds the General Motors Foundation Centennial Teaching Fellowship in Electrical Engineering. He is an active member of the University of Texas Microelectronics Research Center and Electrical Engineering Research Laboratory.

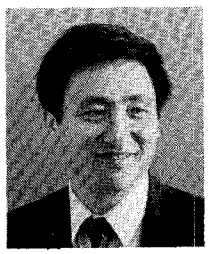

Tatsuo Itoh (S'69–M'69–SM'74–F'82) received the Ph.D. degree in electrical engineering from the University of Illinois, Urbana, in 1969.

From September 1966 to April 1976, he was with the Electrical Engineering Department, University of Illinois. From April 1976 to August 1977, he was a Senior Research Engineer in the Radio Physics Laboratory, SRI International, Menlo Park, CA. From August 1977 to June 1978, he was an Associate Professor at the University of Kentucky, Lexington. In July 1978, he joined the faculty at the University of Texas at Austin, where he is now a Professor of Electrical Engineering and Director of the Electrical Engineering Research Laboratory. During the summer of 1979, he was a guest researcher at AEG-Telefunken, Ulm, West Germany. Since September 1983, he has held the Hayden Head Centennial Professorship of Engineering at the University of Texas. In September 1984, he was appointed Associate Chairman for Research and Planning of the Electrical and Computer Engineering Department. He also holds an Honorary Visiting Professorship at the Nanjing Institute of Technology, China.

Dr. Itoh is a member of Sigma Xi and of the Institute of Electronics and Communication Engineers of Japan. He is a member of Commission B and Chairman of Commission D of USNC/URSI. He served as the Editor of the IEEE TRANSACTIONS ON MICROWAVE THEORY AND TECHNIQUES for the years 1983–1985. He serves on the Administrative Committee of the IEEE Microwave Theory and Techniques Society. Dr. Itoh is a Professional Engineer registered in the state of Texas.